Zinc Oxide Nanostructures and High Electron Mobility Nanocomposite Thin Film Transistors

Flora M. Li, Gen-Wen Hsieh, Sharvari Dalal, Marcus C. Newton, James E. Stott, Pritesh Hiralal, Arokia Nathan, Paul A. Warburton, Husnu Emrah Unalan, Paul Beecher, Andrew J. Flewitt, Ian Robinson, Gehan Amaratunga, and William I. Milne

***Abstract*—This paper reports on the synthesis of zinc oxide (ZnO) nanostructures and examines the performance of nanocomposite thin-film transistors (TFTs) fabricated using ZnO dispersed in both n- and p-type polymer host matrices. The ZnO nanostructures considered here comprise nanowires and tetrapods and were synthesized using vapor phase deposition techniques involving the carbothermal reduction of solid-phase zinc-containing compounds. Measurement results of nanocomposite TFTs based on dispersion of ZnO nanorods in an n-type organic semiconductor ([6, 6]-phenyl-C_{61}-butyric acid methyl ester) show electron field-effect mobilities in the range 0.3–0.6 $cm^2V^{-1}s^{-1}$, representing an approximate enhancement by as much as a factor of 40 from the pristine state. The on/off current ratio of the nanocomposite TFTs approach 10^6 at saturation with off-currents on the order of 10 pA. The results presented here, although preliminary, show a highly promising enhancement for realization of high-performance solution-processable n-type organic TFTs.**

***Index Terms*—High electron mobility, nanocomposite thin-film transistors (TFTs), nanowires (NWs), organic semiconductors, tetrapods, Zinc Oxide (ZnO).**

I. Introduction

NANOSCALE crystalline structures such as nanowires (NWs) and nanotubes are the topic of extensive study as their unique properties have potential for use in novel optical and electronic applications. The increasing need to make smaller device structures with enhanced functionality has led the move away from conventional top–down lithographic approaches toward the utilization of self-assembled nanoscale structures. Moreover, the unique morphologies exhibited by many nanocrystals make them ideal for various applications including gas sensors [1], photodetectors [2]–[4], light emitters [5]–[7], transistors [8], [9], high-frequency oscillators [10], interconnects [7], [11], and waveguides [12].

Manuscript received April 30, 2008; revised August 15, 2008. Current version published October 30, 2008. G.-W. Hsieh was supported by the National Science Council Taiwan through NSC-095-SAF-I-564-025-TMS. The review of this paper was arranged by Editor M. J. Kumar.

F. M. Li, G.-W. Hsieh, S. Dalal, P. Hiralal, H. E. Unalan, P. Beecher, A. J. Flewitt, G. Amaratunga, and W. I. Milne are with the Electrical Engineering Division, University of Cambridge, CB3 0FA Cambridge, U.K.

M. C. Newton, J. E. Stott, A. Nathan, P. A. Warburton, and I. Robinson are with London Centre for Nanotechnology, University College London, WC1H 0AH London, U.K. (e-mail: anathan@ucl.ac.uk).

Color versions of one or more of the figures in this paper are available online at http://ieeexplore.ieee.org.

Digital Object Identifier 10.1109/TED.2008.2005180

Zinc oxide (ZnO) is a polar group II–VI semiconductor material with a direct bandgap of 3.37 eV. ZnO also has several advantages over other wide-bandgap semiconductors in that it is amenable to wet chemical etching using bases such as potassium hydroxide and that it is highly resistive to high-energy radiation. ZnO nanoparticles have been widely used in paints, rubber processing, and sunscreen lotions, while their polycrystalline forms have been used for more high-tech uses such as phosphors, piezoelectric transducers, varistors, and transparent conducting films [13]. Over the past decade, progress in developing single-crystal bulk ZnO and recent results in growing p-type material have brought ZnO's promise as a wide-bandgap semiconductor to the forefront. There is currently a vibrant research effort into ZnO with the hope of creating new kinds of devices such as spin-polarized light-emitting diodes (LEDs) [14] and carrier-mediated ferromagnetism for magnetic storage [15]. ZnO films show n-type conductivity that is often attributed to the presence of H ions and Zn interstitials [16], coupled with the fact that the broad conduction-band minimum in this material results in the charge neutrality level being above the middle of the bandgap [17]. Although ZnO can be reliably produced in any conductivity ranging from semi-insulating piezoelectric material to strongly n-type material exhibiting metallic conduction, p-type material is far more difficult to achieve [18]. Having already been the main reason for past derailments of interest in ZnO, the pursuit of p-type ZnO material, or of heterostructures circumventing the need for p-ZnO material, constitutes a significant research effort.

ZnO also has a large exciton binding energy of 60 meV, which is more than twice that of GaN and much greater than thermal energies at room temperature (25 meV). This allows ZnO to provide stable band-edge ultraviolet (UV) emission at room temperature via an exciton recombination process as opposed to the significantly less efficient electron–hole plasma process employed in current GaN-based devices. The ability to produce UV light efficiently from ZnO NWs has therefore allowed the investigation of their use in LEDs [19] and NW lasers [1]. GaN can also be used for the production of green, blue–UV, and white LEDs, but zinc oxide has some advantages over GaN such as the availability of high-quality ZnO bulk single crystals and the ability to allow devices to work at, and above, room temperature thanks to its thermal stability to temperatures over 1200 °C [20]. The wide bandgap of ZnO (3.37 eV) offers other potential optoelectronic applications for this material. For example, ZnO NWs can be used to make transparent thin-film transistors (TFTs) [21] and transparent electrodes for flat

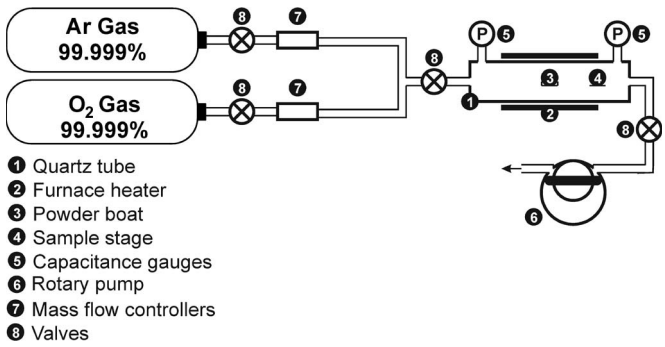

Fig. 1. Diagram of the NW growth setup.

panel displays [22]. They have also been used for making dye-sensitized solar cells [23].

ZnO also forms a large family of self-assembled nanoscale structures ranging from the simple rod shape to flowers and belts [24]–[27]. Quantum-size effects in these nanostructures make them interesting as we can observe and study physical properties different from the bulk material. ZnO nanostructures may be synthesized using a number of techniques, with the most common ones involving a chemical vapor transport process (which can be further subdivided into chemical and physical vapor deposition techniques) [27], [28], solution-based synthesis, and template-based synthesis. Growth using the vapor deposition method involving a carbothermal reaction with zinc oxide and carbon has recently been a prevalent method of growth due to its being safe, inexpensive, and simple [9], [29], [30]. In this method, zinc oxide and carbon powders are mixed together, usually in a ZnO:Zn ratio of 1 : 1 or 1 : 4 by weight. These powders are heated in a tube furnace at high temperatures in the presence of a flow of oxygen gas diluted in argon, and the NW deposits are collected downstream where they have condensed on a substrate placed at a cooler location or on the walls of the tube furnace, as shown in Fig. 1 [30], [31].

Wurtzite ZnO is thermodynamically stable and lacks a center of inversion giving rise to piezoelectricity. Metastable phases, however, often exist in Group IV and compound semiconductors and can be stabilized through epitaxial growth [32], [33]. The coexistence of such phases during synthesis can result in nanocrystals that exhibit more than one crystal structure. This polytypism is what leads to the growth of branched nanostructures in which features of one crystal type branch out from a central core of another. Such branched structures can be seen in II–VI compound semiconductors such as CdSe, CdTe, ZnS, and ZnO. The simplest of these structures is the tetrapod, which consists of four ZnO nanorods joined at tetrahedral angles. This work has focused mainly on the study of devices formed from ZnO nanorods and tetrapods.

While there have been significant advances reported for the synthesis of ZnO nanostructures, their solution processability in the form of nanocomposite materials for device fabrication is less known. Preliminary reports of TFTs based on ZnO nanorods and tetrapods dispersed in a p-type poly[2-mehoxy, 5-(-ethylhexyloxy)-1, 4-phenylene vinylene] polymer matrix [34] showed significant increase in hole field-effect mobility, with values ranging from 10^{-4} $\mathrm{cm}^2 \cdot \mathrm{V}^{-1} \cdot \mathrm{s}^{-1}$ in the pristine state to 0.15 $\mathrm{cm}^2 \cdot \mathrm{V}^{-1} \cdot \mathrm{s}^{-1}$ in the presence of ZnO.

In this paper, preliminary characterization of TFTs based on a dispersion of ZnO nanorods in an n-type polymer semiconductor, [6, 6]-phenyl-C_{61}-butyric acid methyl ester (PCBM), is reported. The TFTs yield electron field-effect mobilities up to 0.56 $\mathrm{cm}^2 \cdot \mathrm{V}^{-1} \cdot \mathrm{s}^{-1}$ with an approximate enhancement by a factor of 40 compared with pristine PCBM. TFTs based on ZnO tetrapods dispersed in the p-type polymer semiconductor poly(3-hexyl-thiophene) (P3HT) are also discussed.

II. Materials Growth and Characterization

A. ZnO NWs

In this paper, ZnO nanostructures were deposited by vapor phase deposition using a carbothermal reaction between ZnO and carbon powder, as described in Section I. For this type of synthesis, a substrate was cleaned, and a thin layer (1–2 nm) of catalyst metal, such as gold or silver, was deposited using a thermal evaporator or sputter coater. The catalyst layer is important as both the type of metal and its thickness can control subsequent NW growth. The NW synthesis took place in an 80-cm quartz tube with a 2.5-cm diameter inside a Carbolite tube furnace, as shown schematically in Fig. 1. The system was pumped using a rotary pump which produced a base pressure of $\sim 3 \times 10^{-2}$ mbar. Capacitance diaphragm pressure gauges were attached both upstream and downstream of the quartz tube to measure growth pressure. The source powder was placed in the quartz tube with the substrates a specific distance downstream from the source. The furnace coils create a temperature gradient down the length of the furnace. A gas mixture of oxygen diluted in argon, or purified air, regulated by mass flow controllers is subsequently flowed into the tube. The pump is throttled to adjust the growth pressure. The source temperature in the center of the furnace is increased to 1000 °C at a ramp rate of 1 $\mathrm{K} \cdot \mathrm{s}^{-1}$ and is then maintained at that temperature from anywhere between 1 and 90 min. After the deposition, the pumping side and air inlet side are switched to reverse any gas flow and thereby prevent further growth while the furnace is left to cool. NW density, alignment, length, and diameter can be controlled using variables such as the growth temperature, pressure, flow rate, and time. NW growth was demonstrated on several types of substrates such as sapphire, gallium nitride, zinc oxide, and silicon.

The NWs were initially studied by scanning electron microscopy (SEM) [FEI Philips XL30 sFEG]. Fig. 2 shows an SEM image of ZnO NWs grown on a sapphire substrate. Clear vertical alignment of the NWs is observed, which is attributed to the fact that a-plane sapphire has a similar lattice constant to ZnO. Gallium nitride is also lattice matched to ZnO, and aligned growth also occurs on this substrate material (see Fig. 2).

The crystalline structure of the NWs was measured using a JEOL 3011 transmission electron microscope (TEM). Fig. 3(a) shows the tip of the NWs. No catalyst metal was seen at the tip of the NWs, suggesting that growth takes place from the base of the wires. The NWs appear to have a hexagonal cross section which is consistent with their wurtzite structure. Fig. 3(b) shows a high-resolution TEM (HRTEM) image of a typical ZnO NW. Planes of atoms perpendicular to the axial direction of the NW with a separation of 0.26 nm are seen, which corresponds to

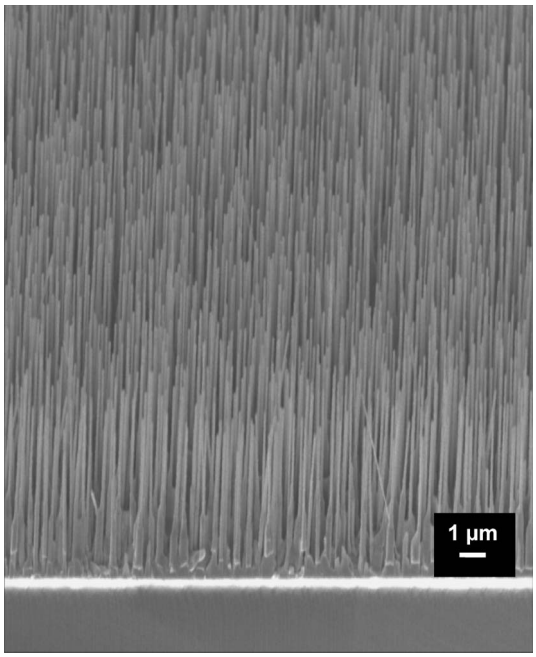

Fig. 2. Aligned ZnO NWs on the sapphire substrate.

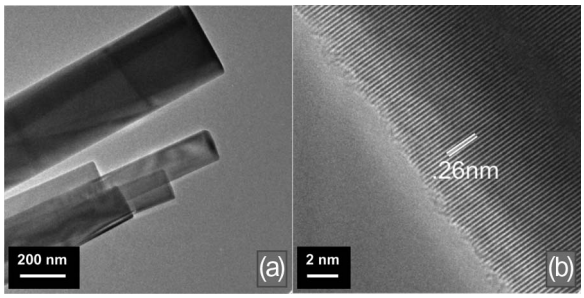

Fig. 3. (a) TEM of several NWs showing flat catalyst-free tips. (b) HRTEM image of ZnO NW showing 0.26-nm spacing corresponding to (0002) growth direction.

the distance between two (0002) planes, confirming that growth occurs in the c-axis [0001] direction. X-ray diffraction (XRD) spectra were taken by a Philips PW1820 diffractometer, and the results for unaligned NWs are shown in Fig. 4(a). The peaks are consistent with the hexagonal wurtzite phase of ZnO. Fig. 4(b) shows the XRD spectrum for a sample of aligned NWs. Only two peaks are now observed, namely, a very sharp (0002) peak and a less intense (0004) peak. This confirms both the growth direction and excellent alignment [35]. Auger electron spectroscopy was performed using a PHI680 Auger nanoprobe whose beam can be focused down to 13 nm, making it ideal for use on nanostructures. This revealed that the composition of the NW grown at 3 mbar with purified air is composed of 45% O and 55% Zn, making the NWs slightly oxygen deficient compared with the ideal ZnO stoichiometry. Electrical measurements show that NWs grown with air as the carrier gas have a resistivity of 11.3 $\Omega \cdot$ cm, whereas those grown with 2% O_2 in Ar have a resistivity of 0.17 $\Omega \cdot$ cm. Purified air has a significantly higher oxygen partial pressure than the 2% O_2 in Ar, and so NWs grown in the latter environment are likely to be even more oxygen deficient, and therefore more metallicike in conduction, resulting in a significantly lower resistivity.

X-ray photoemission spectroscopy (XPS) measurements were made on the NWs using a VG ESCALAB MK-II photoelectronic energy spectrometer. Two main oxygen binding peaks are observed, as shown in Fig. 5. The peak at 530 eV is assigned to Zn–O bonding, while the peak at 532 eV is believed to be due to OH species, which are most likely located at the NW's surface [36].

The photoluminescence (PL) spectrum of the NWs is shown in Fig. 6. A sharp peak is observed at $\sim$3.2 eV, which is believed to be due to the transition of free electrons into acceptor states (e, A^0 transitions) caused by the unintentional incorporation of nitrogen substitutionally for oxygen in the ZnO structure (N_O defects) [37]. A broad green PL peak is also observed close to 2.4 eV. The origin of this is more controversial, but the lack of structure suggests that this is most likely caused by oxygen vacancies (V_O defects) which are known to be common in ZnO material and are particularly likely in the metal-rich NWs produced in this paper [20]. ZnO is known to readily adsorb atoms and, particularly, oxygen-containing species [38]–[40]. These absorbed species are known to affect the surface conductivity of the NWs. It is believed that this occurs because absorption takes place at vacancy defect sites on the NW's surface. A charge transfer then occurs, resulting in the absorbed species gaining a negative charge, and this causes the formation of a depletion layer at the surface of the n-type ZnO. Exposure to UV light causes the formation of electron–hole pairs in the ZnO, allowing the negative charge on the absorbed oxygen species to be removed and desorption to occur, resulting in a restoration of the NW's electrical characteristics [38]. A similar effect has been observed on the surface of thin films of ZnO [41]. Whereas this behavior has been successfully utilized for sensor applications [42]–[44], problems arising from formation of nonohmic contacts and instability in threshold voltage of ZnO NW FETs or decrease in mobility of ZnO NW networks can limit its application.

ZnO is intrinsically n-type, and creating p-type ZnO has been one of the greatest material challenges in this area. The major problem is that impurities tend to be compensated by defects of the opposite charge rather than forming a dopant with a shallow state in the bandgap [17]. Consequently, although p-type ZnO thin films have been reported, the doping is often unstable, and the material can revert to being n-type [20]. However, p-type ZnO NWs have been recently synthesized by using a simple chemical vapor deposition method using phosphorus pentoxide (P_2O_5) as the dopant source [45].

B. ZnO Tetrapods

As with ZnO nanorod growth, tetrapods are most commonly synthesized through a carbothermal reduction process within a horizontal tube furnace using a similar setup to that shown in Fig. 1. Nucleation and growth of ZnO tetrapods, however, proceed without the aid of a catalyst. Synthesis by heating Zn metal is also reported but often yields less uniform growth. In this paper, the source material—a mixture of graphite (C) and a zinc carbonate $(ZnCO_3 \bullet 2Zn(OH)_2 \bullet H_2O)$—is placed in the center of the furnace where the temperature is in the range of 600 °C–700 °C to collect the growth constituents. The furnace is then heated to 900 °C in the region of the source

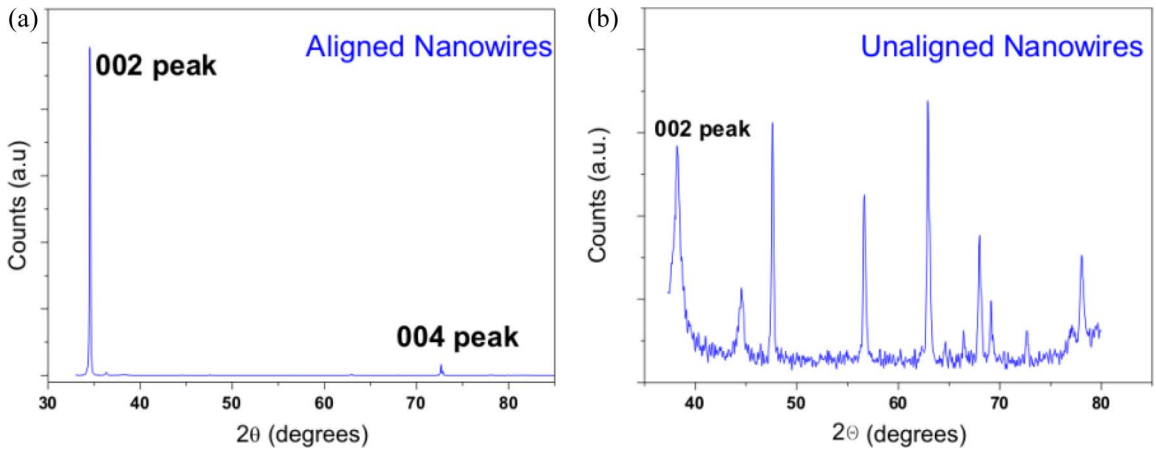

Fig. 4. XRD spectra of (a) aligned and (b) unaligned NW samples.

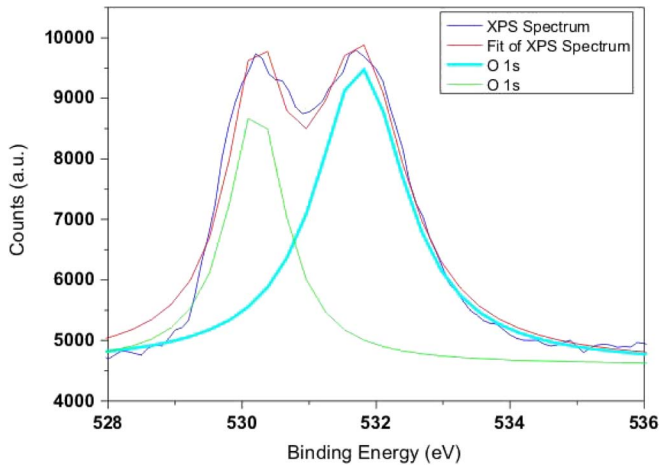

Fig. 5. XPS spectrum showing two oxygen 1-s peaks possibly corresponding to oxygen defects on surface.

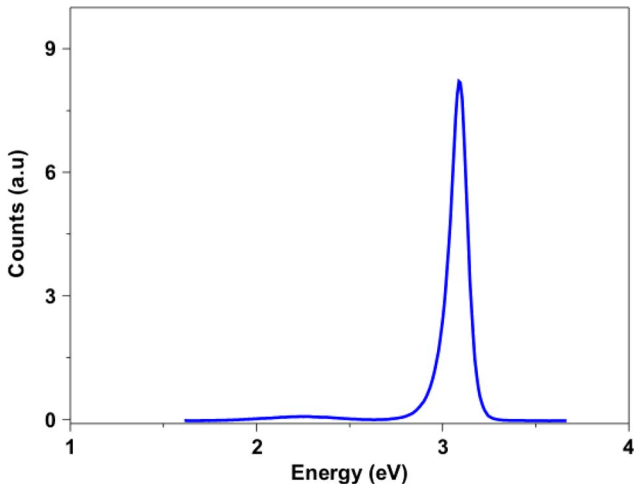

Fig. 6. Typical PL spectrum showing a low-oxygen defect peak.

material in a flow of either Ar or N_2 with an O_2 partial pressure of 0.5%–5% of the total pressure. A carbothermal reduction process releases supersaturated Zn into the oxygen which condenses downstream in the form of tetrapod nanocrystals.

Fig. 7 shows an example of ZnO tetrapods that we have synthesized. Control over the size and morphology of the nanocrystals is achieved by varying the growth parameters such as the O_2 content and substrate temperature during synthesis [46].

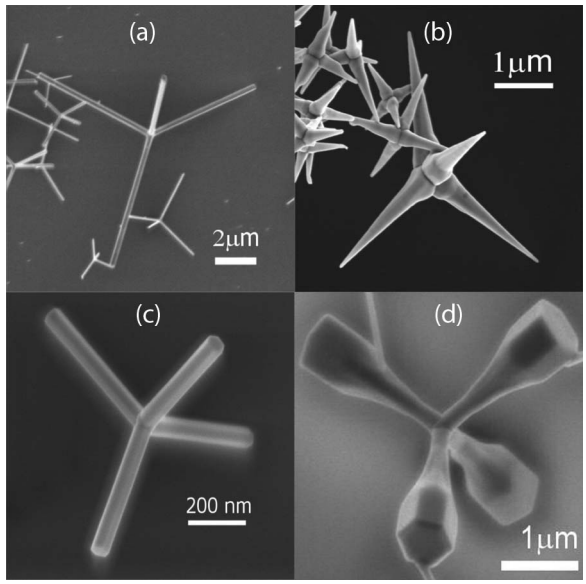

Fig. 7. SEM images of ZnO tetrapod nanocrystals. At low oxygen content ($<$ 5 sccm), (b) tetrapods are grown with needle-shaped arms. At low oxygen content, (c) smaller tetrapods tend to form at lower temperature regions and regain their cylindrical arm shape. As the oxygen content is increased to 25 sccm, (a) ZnO tetrapods are found with increased arm lengths and diameters. At higher temperature regions, (d) tetrapods with trumpet-shaped arms form under high oxygen content.

Room-temperature PL measurements were carried out on ZnO tetrapod clusters and isolated individual ZnO tetrapods to better understand the defect and impurity states in this material. Light from a 325-nm He–Cd continuous-wave laser was used as an excitation source and was focused onto the sample surface. Fig. 8 shows the PL spectrum for an isolated individual tetrapod and a cluster of tetrapod nanocrystals. As with the ZnO NWs, a sharp (e, A^0) transition peak is observed at ~3.2 eV and a broad V_O defect peak at ~2.4 eV. Randomly orientated tetrapod clusters exhibit emission dominated by the broad peak at 2.4 eV, while the spectrum of the isolated tetrapod is dominated by the peak centered at 3.2 eV. ZnO tetrapod nanocrystals orientate spontaneously with one arm normal to the substrate. As the single optical axis is aligned along the arm, band-edge emission

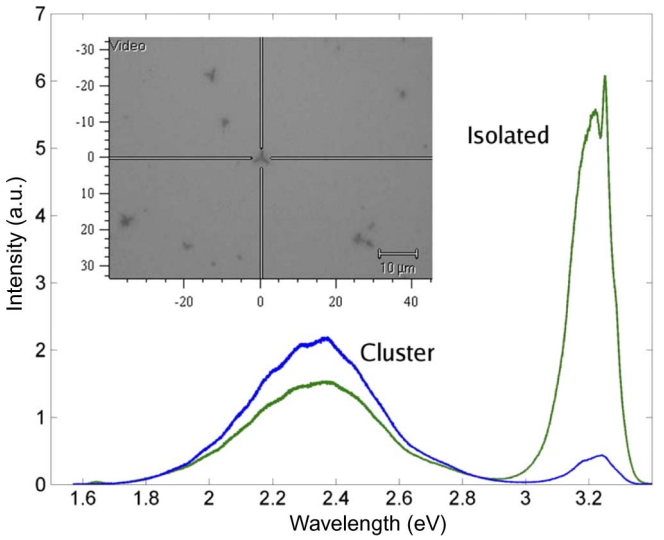

Fig. 8. Room-temperature PL of (a) ZnO tetrapod cluster and (b) isolated ZnO tetrapod. The inset shows an optical image of a ZnO tetrapod at the center of the crosshair.

is expected to be most intense in this direction. Enhancement of the UV peak for an isolated ZnO tetrapod is therefore understood, as the UV emission points toward the detector normal to the substrate. In the case of the V_O defect peak at ~2.4 eV, however, the greater density of ZnO tetrapods in the clustered sample results in a more intense emission at this photon energy.

III. TFTs

Bottom-gate bottom-contact TFTs featuring stamped or solution-dispersed ZnO nanostructure networks with a solution-processable organic-semiconductor host matrix were fabricated on highly doped silicon substrate while also acted as a common gate. Thermally grown silicon dioxide (SiO_2) or plasma-enhanced chemical-vapor-deposited silicon nitride (SiN_x) was used for the gate dielectric layer. Thermally evaporated chromium (Cr) or sputtered molybdenum (Mo) formed the source and drain contacts.

Electrical characterization of the TFTs was carried out with a Keithley 4200-SCS parameter analyzer or with an Agilent B1500A semiconductor device analyzer. From the measured transfer characteristic (I_D versus V_{GS}), the transconductance (g_m), threshold voltage (V_T), and effective field-effect mobility (μ_{FE}) of the TFTs were extracted using the following expressions governing MOSFET operation in the linear and saturation regions:

$$I_D = \mu_{FE} C_i \frac{W}{L}(V_{GS} - V_T)V_{DS}$$
$$g_m = \frac{\partial I_D}{\partial V_{GS}} = \mu_{FE} C_i \frac{W}{L} V_{DS} \quad (1)$$
$$I_{D,sat} = \frac{1}{2}\mu_{FE} C_i \frac{W}{L}(V_{GS} - V_T)^2$$
$$g_m = \frac{\partial I_{D,sat}}{\partial V_{GS}} = \mu_{FE} C_i \frac{W}{L}(V_{GS} - V_T). \quad (2)$$

Here, I_D is the drain current, V_{GS} is the gate–source voltage, V_{DS} is the gate–source voltage, C_i is the gate dielectric capacitance per unit area, W is the channel width, and L is the channel length.

A. N-Type Nanocomposite OTFTs With ZnO NW Networks

Large-area and flexible electronics is a rapidly expanding research area, where much attention has been focused on organic semiconductors. Organic semiconductors have attracted much interest by virtue of their solution processability [47]–[49]. However, the field-effect mobility and stability of organic TFTs (OTFTs) may limit their widespread adoption. While OTFTs often exhibit reasonably high on/off current ratios, attempts to improve their mobilities (typically < 0.1 $cm^2 \cdot V^{-1} \cdot s^{-1}$) and stability remain a subject of ongoing research [47]. These limitations of organic materials have prompted the pursuit of alternative material systems and options for use in large-area and flexible electronics.

One-dimensional nanostructures, such as carbon nanotubes (CNTs) and NWs, present feasible alternatives to fulfill these motivations; these nanostructures can be used as the sole material in a device structure or can be implemented as a complement to organic semiconducting material to form nanocomposite-based devices [46], [51]–[55]. Several groups have recently considered CNTs for fabrication of solution-processed p-type composite TFTs; they were incorporated into P3HT and poly[5, 5'-bis(3-dodecyl-2-thienyl)-2, 2'-bithiophene] (PQT-12) which are organic semiconducting polymers [46], [52], [55]. However, there are few reports concerning solution-processed n-type OTFTs with high field-effect electron mobility [56]–[60]. Here, we first report a means of enhancing n-type OTFT devices by introducing random arrays of stamped semiconducting ZnO NWs. An n-type solution-processed organic semiconductor, PCBM, shown in Fig. 9(a) is utilized as the organic host matrix in this paper. With pristine PCBM, typical field-effect electron mobility is 10^{-3}–10^{-2} $cm^2 \cdot V^{-1} \cdot s^{-1}$ [58]–[60]. Our preliminary results reveal that the effective field effect mobilities of ZnO nanowire–PCBM composite TFT devices are increased by 20–40 times compared to pristine PCBM OTFT devices, while the on/off current ratio is maintained in the range of 10^5.

ZnO NWs are synthesized, as previously described in Section II-A. The growth was performed for 30 min at 3 mbar at 850 °C on a silicon substrate. The NWs were subsequently transferred onto highly doped silicon substrates covered by 150-nm-thick SiO_2 insulating layer by means of a contact stamping method [61]. The density of NWs transferred onto the SiO_2 surface can be changed either by adjusting the applied force during the stamping process or by varying the number of as-grown NWs on the initial substrate that was stamped onto the same area. A lubricant such as poly-L-lysine (Aldrich) was sometimes used to increase the density of transferred NWs. An SEM photograph of stamped ZnO NWs is shown in Fig. 9(b). Source and drain contact patterns, defined by conventional photolithography, used 50-nm-thick chromium (Cr) electrodes thermally evaporated onto the substrates of stamped ZnO NWs. Devices were bottom gate bottom contact geometry, as shown schematically in Fig. 9(c), with channel length L of 10 μm and width W of 30 μm.

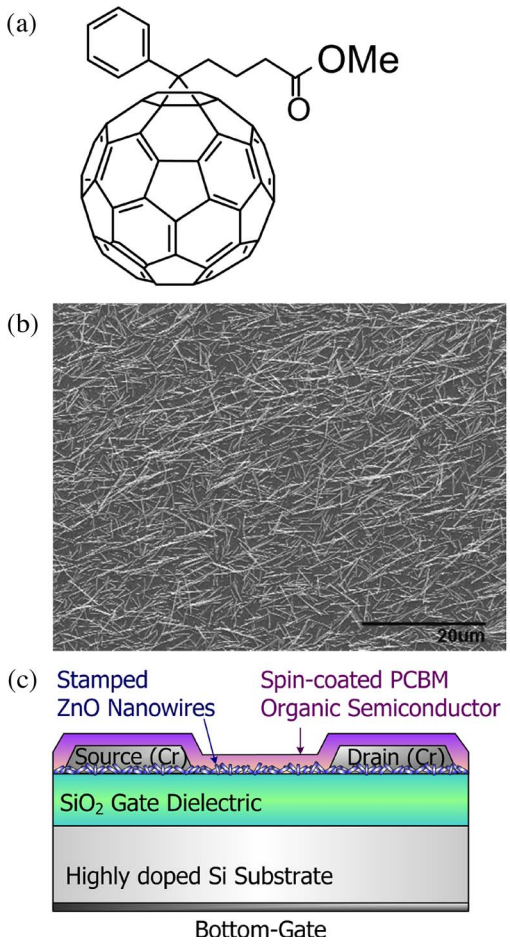

Fig. 9. (a) Chemical structure of PCBM. (b) Network of stamped ZnO NWs with an average length of 5–7 μm and a diameter of 50–100 nm (Scale bar: 20 μm). (c) Schematic cross section of the composite ZnO–PCBM TFT structure employed in this paper.

Prior to the deposition of organic-semiconductor layer, the entire surface of stamped substrates with electrodes was treated with hexamethyldisilazane (Aldrich). PCBM (99.9%, Aldrich), in a 10-mg $\cdot$ mL^{-1} chloroform solution, was spin coated (500 r/min for 5 s and then 1700 r/min for 60 s) onto the substrates containing ZnO NWs and Cr electrodes inside a N_2 glove box. Pristine PCBM devices were also fabricated by the same manner without the ZnO stamping process. The devices were then annealed at 100 °C in vacuum (10^{-4} mbar) for 12 h. Electrical characterization of the transistor devices was performed under a N_2-purged atmosphere at room temperature and in the dark. The performance of these composite ZnO–PCBM TFTs is presented alongside that of the pristine PCBM OTFTs.

The output characteristics for a pristine PCBM device for different gate voltages are shown in Fig. 10(a). The $I_{\rm DS}$–$V_{\rm DS}$ curves clearly resemble those of a typical n-type field-effect transistor, where drain current increases and saturates when the positive drain voltage is increased. Fig. 10(b) shows the output characteristics for a composite ZnO–PCBM device. The $I_{\rm DS}$ increases up to 15 μA at $V_{\rm DS} = 50$ V and $V_{\rm GS} = 50$ V, which is about 150 times higher than that of the pristine PCBM device. We also note a small negative $I_{\rm DS}$ observed at low source/drain voltages and high gate voltages in the pristine PCBM device. We believe that it is associated with a Poole–Frenkel electron–hole generation mechanism in which the drain is now collecting a hole current. This generation mechanism is strongly dependent on the electric field and thus grows with increasing $V_{\rm GS}$. Therefore, the PCBM, although an n-type material, shows ambipolar behavior [59].

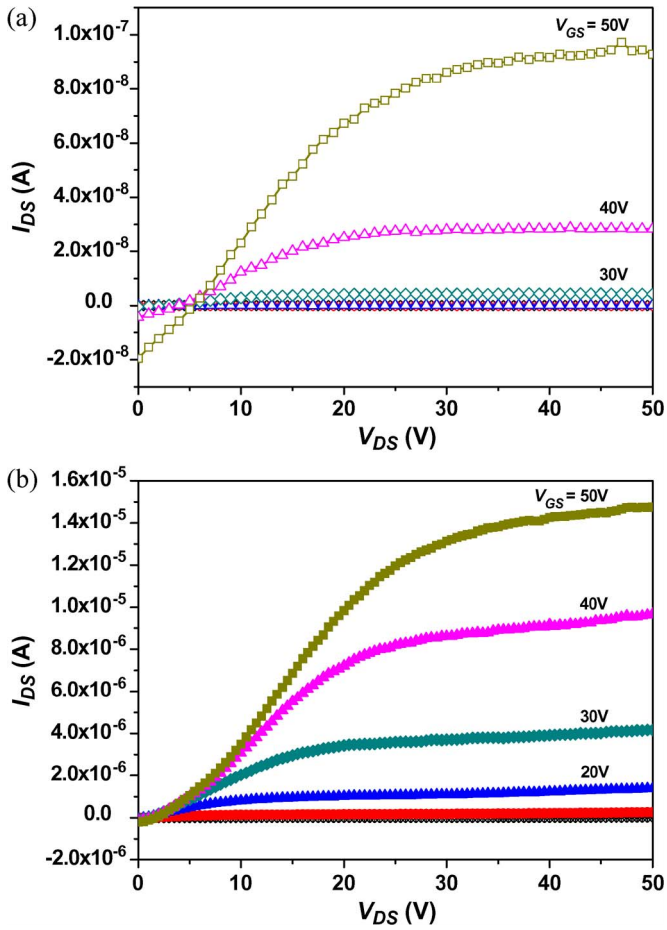

Fig. 10. Output $I_{\rm DS}$–$V_{\rm DS}$ characteristics of (a) the pristine PCBM TFT device and (b) the composite ZnO–PCBM TFT device.

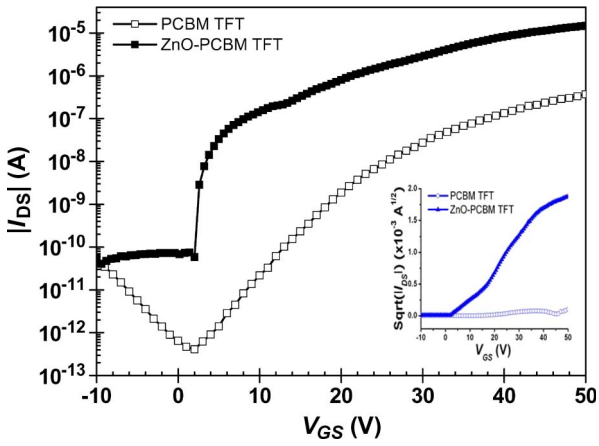

Fig. 11. Transfer $I_{\rm DS}$–$V_{\rm GS}$ characteristics of pristine PCBM and ZnO–PCBM TFT devices in the saturation regime at $V_{\rm DS} = 40$ V. The inset shows the $I_{\rm DS}^{1/2}$–$V_{\rm GS}$ characteristics in the linear regime at $V_{\rm DS} = 10$ V.

Fig. 11 shows the transfer characteristics of pristine PCBM TFT and ZnO–PCBM TFT devices. In the saturation regime ($V_{\rm DS} = 40$ V), the field-effect mobility is calculated by plotting

TABLE I
FIELD-EFFECT MOBILITY ($\mu_{\rm FE}$), ON/OFF CURRENT RATIO, OFF-CURRENT ($I_{\rm OFF}$), THRESHOLD VOLTAGE (V_T), AND SUBTHRESHOLD SWING (S) OF PRISTINE PCBM AND ZnO–PCBM TFT DEVICES AT $V_{\rm DS} = 40$ AND 10 V, RESPECTIVELY

Bias Regime	TFT	μ_{FE} ($cm^2 V^{-1} s^{-1}$)	*ON/OFF Current Ratio*	I_{OFF} (A)	V_T (V)	S ($V\ dec^{-1}$)
$V_{\rm DS}$ = 40 V (saturation)	Pristine PCBM	0.0334	9×10^5	4×10^{-13}	~ 12	4.606
	ZnO-PCBM	0.561	4×10^5	5×10^{-11}	~ 4	0.356
$V_{\rm DS}$ = 10 V (linear)	Pristine PCBM	0.0071	9×10^4	1×10^{-13}	~ 15	2.810
	ZnO-PCBM	0.285	1×10^5	6×10^{-11}	~ 5	0.898

the square root of the drain current versus the gate voltage and fitting the data to (2). The saturation field-effect mobility of pristine PCBM is 0.0334 $\rm cm^2 \cdot V^{-1} \cdot s^{-1}$, and the on/off current ratio is 9×10^5, which are comparable with the results reported in the literature for PCBM devices [58], [60]. For the ZnO–PCBM TFT device, the field-effect mobility is increased to 0.561 $\rm cm^2 \cdot V^{-1} \cdot s^{-1}$, representing an improvement of more than 17 times over the pristine PCBM TFT device. The on/off current ratio remains on the same order in both composite and pristine TFTs. Furthermore, a sharper subthreshold slope is observed in the ZnO–PCBM device. However, the improvements in composite ZnO–PCBM TFTs come with a tradeoff in terms of the off-current and are likely linked to the higher conductivity of ZnO NWs compared with the organic semiconducting matrix. We believe that further process optimization of the ZnO NW conductivity via refined control of the growth process parameters can provide a remedy to suppress the OFF state; this is currently under investigation.

When the transfer characteristics measured are close to the linear regime ($V_{\rm DS} = 10$ V), shown in the inset of Fig. 11, the field-effect mobility of the pristine PCBM TFT extracted from transconductance measurements, based on (1), is 0.0071 $\rm cm^2 \cdot V^{-1} \cdot s^{-1}$, and the on/off current ratio is 9×10^4. In contrast, the composite ZnO–PCBM TFT exhibits mobility of 0.285 $\rm cm^2 \cdot V^{-1} \cdot s^{-1}$ and on/off current ratio of 1×10^5. The field-effect mobility is improved markedly by 40 times by incorporating ZnO NWs into the organic matrix.

The field-effect mobility, on/off current ratio, off-current, threshold voltage, and subthreshold slope of pristine PCBM and ZnO–PCBM TFT devices in the saturation and linear regimes are summarized in Table I. The measurement results of composite ZnO–PCBM TFTs are found to exhibit superior performance compared with those of pristine PCBM TFTs. The incorporation of ZnO NWs produces higher on-current ($\sim$10 μA), higher mobility, steeper subthreshold slope, and reduced threshold voltage (closer to zero). The increase in the field-effect mobility is probably due to the superior semiconducting properties of the ZnO. In the most simplistic form, the NWs could be viewed as conducting bridges which serve to enhance electron transport between crystals in the PCBM film. Furthermore, there may be an increased number of charge carriers in the transport channel. For a better understanding of the role of each material, further experiments will examine the effect of different network densities of ZnO NWs on the field-effect characteristics. Experiments will also need to be conducted to optimize device properties and to examine the stability of composite TFTs relative to OTFTs. In addition, ZnO NW networks without organic materials are being evaluated for TFT performance, and these results will be presented elsewhere.

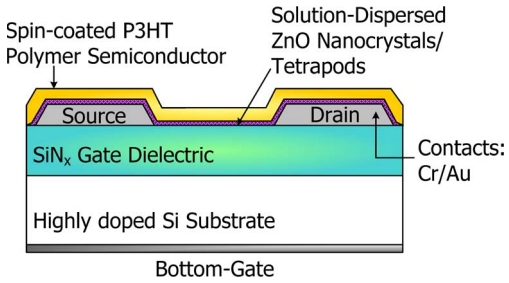

Fig. 12. Cross-sectional structure of the bottom-gate bottom-contact spin-coated nanocomposite ZnO/P3HT TFT device.

Overall, the results reported here show a promising approach for integrating 1-D nanostructures with solution-processed organic semiconductors to enhance TFT performance for large-area electronic applications.

B. P-Type Nanocomposite OTFTs With ZnO Tetrapods

While we report n-type OTFT structures with enhanced electron transport by incorporation of ZnO NWs, there are few reports of similar effects in p-type host materials, with one study suggesting that the p-channel enhancement effect is the result of a reduction in the density of traps caused by ZnO tetrapods [34]. Preliminary experiments suggest that the incorporation of ZnO nanostructures can enhance the mobility and maximum on-current for a given p-type polymer device. However, challenges remain to be overcome in achieving the overall device characteristics exhibited in similar n-type devices, with increased off-currents degrading device performance.

ZnO nanoparticles (20 nm, Sigma Aldrich) and tetrapods synthesized, as described in Section II-B, were dispersed in a chlorobenzene solution of P3HT (Rieke Metals), and transistors were fabricated by spin coating the ZnO/polymer nanocomposite on a prepatterned substrate, with a bottom-gate transistor structure being shown in Fig. 12. Compared to pristine polymer devices, the incorporation of ZnO nanoparticles resulted in an increase in the on-current and mobility in the saturation regime for the composite TFTs. However, this was accompanied by a rise in the off-current. Experiments to fabricate ZnO/polymer composite TFTs with ZnO tetrapods were less successful, due to difficulties in fully dispersing ZnO tetrapods in the polymer semiconductor solution prior to deposition. A sonic bath was used to disperse the tetrapods before mixing with polymer in

solution; however, this was insufficient to promote full dispersion, with a clustering of tetrapods being visible.

An alternative method is to disperse ZnO tetrapods before spin coating a polymer film from solution. A detailed study here is necessary to assess the effect of the ZnO at the dielectric interface, the surface treatment of which can lead to significant enhancement of performance [62]. Should the ZnO interfere with the organization of the polymer at the dielectric interface, it may well reduce the effectiveness of surface treatments.

Another consideration is the size of ZnO tetrapods; channel lengths are on the order of 10 μm, whereas the tetrapods are 1–2 μm in length, and the polymer films are several hundred nanometers in thickness. Since film thicknesses rarely approach the size of the tetrapods, the device characteristics can no longer be considered simply in terms of a channel formed at the dielectric interface; tetrapod orientation also becomes important. It is hoped that the introduction of smaller tetrapods will improve uniformity of characteristics, and reduce dependence on geometry and anisotropy, as the size becomes comparable with polymer film thickness at several hundred nanometers.

IV. Conclusion

This work demonstrated the synthesis of ZnO nanorods and tetrapods and fabrication of nanocomposite TFTs based on dispersion of the nanostructures in n- and p-type organic-semiconductor host matrices. Measurement results of transfer and input–output characteristics for n-type nanocomposite transistors yield promising results with respect to device mobility, on/off current ratio, and off-current. Although the results presented here are preliminary, the observed enhancement in device performance from the pristine state demonstrates the promise for high-performance solution-processable n-type OTFTs. While the enhancement in the presence of the nanostructures is significant, we believe that there is room for improvement. Further work will address the challenges associated with refining the synthesis procedure for improved control of size and impurity doping of the ZnO tetrapods. In particular, our present results of p-type nanocomposite TFTs have been less successful in terms of device characteristics. This may be attributed to a failure of the relatively large (submicrometer-sized) tetrapods to fully disperse in the polymer solution prior to deposition, despite sonication. However, we expect to see improved results with smaller tetrapods. Work along these lines is currently in progress.

Acknowledgment

F. M. Li would like to thank the support from the Ontario Centers of Excellence, Canada. G.-W. Hsieh would like to thank the support of Cambridge Overseas Trust.

References

[1] C. Xiangfeng, J. Dongli, A. B. Djurisic, and Y. H. Leung, "Gas-sensing properties of thick film based on ZnO nano-tetrapods," *Chem. Phys. Lett.*, vol. 401, no. 4–6, pp. 426–429, Jan. 2005.

[2] Y. Heo *et al.*, "Pt/ZnO nanowire Schottky diodes," *Appl. Phys. Lett.*, vol. 85, no. 15, pp. 3107–3109, Oct. 2004.

[3] J. Wang, M. S. Gudiksen, X. Duan, Y. Cui, and C. M. Lieber, "Highly polarized photoluminescence and photodetection from single indium phosphide nanowires," *Science*, vol. 293, no. 5534, pp. 1455–1457, Aug. 2001.

[4] Z. Fan *et al.*, "Photoluminescence and polarized photodetection of single ZnO nanowires," *Appl. Phys. Lett.*, vol. 85, no. 25, pp. 6128–6130, Dec. 2004.

[5] R. Konenkamp, R. C. Word, and C. Schlegel, "Vertical nanowire light-emitting diode," *Appl. Phys. Lett.*, vol. 85, no. 24, pp. 6004–6006, Dec. 2004.

[6] X. Duan, Y. Huang, R. Agarwal, and C. Lieber, "Single-nanowire electrically driven lasers," *Nature*, vol. 421, no. 6920, pp. 241–245, Jan. 2003.

[7] X. Duan, Y. Huang, Y. Cui, J. Wang, and C. M. Lieber, "Indium phosphide nanowires as building blocks for nanoscale electronic and optoelectronic devices," *Nature*, vol. 409, no. 6816, pp. 66–69, Jan. 2001.

[8] Y. Cui, Z. Zhong, D. Wang, W. Wang, and C. Lieber, "High performance silicon nanowire field effect transistors," *Nano Lett.*, vol. 3, no. 2, pp. 149–152, 2003.

[9] M. H. Huang, S. Mao, H. Feick, H. Yan, Y. Wu, H. Kind, E. Weber, R. Russo, and P. Yang, "Room-temperature ultraviolet nanowire nanolasers," *Science*, vol. 292, no. 5523, pp. 1897–1899, Jun. 2001.

[10] R. S. Friedman, M. C. McAlpine, D. S. Ricketts, D. Ham, and C. M. Lieber, "Nanotechnology: High-speed integrated nanowire circuits," *Nature*, vol. 434, no. 7037, p. 1085, Apr. 2005.

[11] J. Li, Q. Ye, A. Cassell, H. T. Ng, R. Stevens, J. Han, and M. Meyyappan, "Bottom–up approach for carbon nanotube interconnects," *Appl. Phys. Lett.*, vol. 82, no. 15, pp. 2491–2493, Apr. 2003.

[12] M. Law *et al.*, "Nanoribbon waveguides for subwavelength photonics integration," *Science*, vol. 305, no. 5688, pp. 1269–1273, Aug. 2004.

[13] C. Jagadish and S. J. Pearton, *Zinc Oxide Bulk, Thin Films and Nanostructures: Processing, Properties and Applications*. Amsterdam, The Netherlands: Elsevier, 2006.

[14] M. Holub and P. Bhattacharya, "Spin-polarized light-emitting diodes and lasers," *J. Phys. D, Appl. Phys.*, vol. 40, no. 11, pp. R179–R203, Jun. 2007.

[15] K. Ip *et al.*, "Ferromagnetism in Mn- and Co-implanted ZnO nanorods," *J. Vac. Sci. Technol. B, Microelectron. Process. Phenom.*, vol. 21, no. 4, pp. 1476–1481, Jul. 2003.

[16] D. C. Look, "Recent advances in ZnO materials and devices," *Mater. Sci. Eng. B*, vol. 80, no. 1, pp. 383–387, Mar. 2001.

[17] J. Robertson, "Disorder, band offsets, and dopability of transparent conducting oxides," *Thin Solid Films*, vol. 516, no. 7, pp. 1419–1425, Feb. 2008.

[18] D. Look and B. Claflin, "P-type doping and devices based on ZnO," *Phys. Stat. Sol. (B)*, vol. 241, no. 3, pp. 624–630, Feb. 2004.

[19] J. Jiao, Z. Z. Zhang, Y. M. Lu, D. Z. Shen, B. Yao, J. Y. Zhang, B. H. Li, D. X. Zhao, X. W. Fan, and Z. K. Tang, "ZnO p-n junction light-emitting diodes fabricated on sapphire substrates," *Appl. Phys. Lett.*, vol. 88, no. 3, p. 031 911, Jan. 2006.

[20] U. Ozgur, I. A. Ya, C. Liu, A. Teke, M. A. Reshchikov, S. Dogan, V. Avrutin, S. J. Cho, and H. Morkoc, "A comprehensive review of ZnO materials and devices," *J. Appl. Phys.*, vol. 98, no. 4, p. 041 301, Aug. 2005.

[21] S. Ju, K. Lee, M. H. Yoon, A. Facchetti, T. J. Marks, and D. B. Janes, "High performance ZnO nanowire field effect transistors with organic gate nanodielectrics: Effects of metal contacts and ozone treatment," *Nanotechnology*, vol. 18, no. 15, p. 155 201, Apr. 2007.

[22] D. S. Ginley and C. Bright, "Transparent conducting oxides," *MRS Bull.*, vol. 25, pp. 15–18, 2000.

[23] M. Law, L. E. Greene, J. C. Johnson, R. Saykally, and P. Yang, "Nanowire dye-sensitized solar cells," *Nat. Mater.*, vol. 4, no. 6, pp. 455–459, Jun. 2005.

[24] Z. L. Wang, "Zinc oxide nanostructures: Growth, properties and applications," *J. Phys., Condens. Matter*, vol. 16, no. 25, pp. R829–R858, Jun. 2004.

[25] Z. L. Wang and J. Song, "Piezoelectric nanogenerators based on zinc oxide nanowire arrays," *Science*, vol. 312, no. 5771, pp. 242–246, Apr. 2006.

[26] Z. L. Wang, "Nanostructures of zinc oxide," *Mater. Today*, vol. 7, no. 6, pp. 26–33, Jun. 2004.

[27] M. C. Newton, S. Firth, T. Matsuura, and P. A. Warburton, "Synthesis and characterisation of zinc oxide tetrapod nanocrystals," *J. Phys. Conf. Ser.*, vol. 26, pp. 251–255, 2006.

[28] M. C. Newton, S. Firth, and P. A. Warburton, "ZnO tetrapod Schottky photodiodes," *Appl. Phys. Lett.*, vol. 89, no. 7, p. 072 104, Aug. 2006.

[29] J. H. Park, Y. J. Choi, and J. G. Park, "Synthesis of ZnO nanowires and nanosheets by an O_2-assisted carbothermal reduction process," *J. Cryst. Growth*, vol. 280, no. 1/2, pp. 161–167, Jun. 2005.

[30] D. Banerjee, J. Y. Lao, D. Z. Wang, J. Y. Huang, Z. F. Ren, D. Steeves, B. Kimball, and M. Sennett, "Large-quantity free-standing ZnO nanowires," *Appl. Phys. Lett.*, vol. 83, no. 10, pp. 2061–2063, Sep. 2003.
[31] J. S. Lee, M. I. Kang, S. Kim, M. S. Lee, and Y. K. Lee, "Growth of zinc oxide nanowires by thermal evaporation on vicinal Si (100) substrate," *J. Cryst. Growth*, vol. 249, no. 1/2, pp. 201–207, Feb. 2003.
[32] A. Ashrafi and C. Jagadish, "Review of zincblende ZnO: Stability of metastable ZnO phases," *J. Appl. Phys.*, vol. 102, no. 7, p. 071 101, Oct. 2007.
[33] S. W. H. Eijt *et al.*, "Formation and stability of rocksalt ZnO nanocrystals in MgO," *Appl. Phys. Lett.*, vol. 91, no. 20, p. 201 906, Nov. 2007.
[34] Z.-X. Xu, V. A. L. Roy, P. Stallinga, M. Muccini, S. Toffanin, H.-F. Xiang, and C.-M. Che, "Nanocomposite field effect transistors based on zinc oxide/polymer blends," *Appl. Phys. Lett.*, vol. 90, no. 22, p. 223 509, May 2007.
[35] L. C. Campos, S. H. Dalal, D. L. Baptista, R. Magalhães-Paniago, A. S. Ferlauto, W. I. Milne, L. O. Ladeira, and R. G. Lacerda, "Determination of the epitaxial growth of zinc oxide nanowires on sapphire by grazing incidence synchrotron X-ray diffraction," *Appl. Phys. Lett.*, vol. 90, no. 18, p. 181 929, Apr. 2007.
[36] L.-J. Meng, C. P. Moreira de Sá, and M. P. dos Santos, "Study of the structural properties of ZnO thin films by X-ray photoelectron spectroscopy," *Appl. Surf. Sci.*, vol. 78, no. 1, pp. 57–61, May 1994.
[37] K. Thonke, T. Gruber, N. Teofilov, R. Schönfelder, A. Waag, and R. Sauer, "Donor–acceptor pair transitions in ZnO substrate material," *Physica B*, vol. 308–310, pp. 945–948, 2001.
[38] Q. H. Li, Y. X. Liang, Q. Wan, and T. H. Wang, "Oxygen sensing characteristics of individual ZnO nanowire transistors," *Appl. Phys. Lett.*, vol. 85, no. 26, pp. 6389–6391, Dec. 2004.
[39] Z. Fan, D. Wang, P.-C. Chang, W.-Y. Tseng, and J. G. Lu, "ZnO nanowire field-effect transistor and oxygen sensing property," *Appl. Phys. Lett.*, vol. 85, no. 24, pp. 5923–5925, Dec. 2004.
[40] O. Schmidt, A. Geis, P. Kiesel, C. G. Van de Walle, N. M. Johnson, A. Bakin, A. Waag, and G. H. Döhler, "Analysis of a conducting channel at the native zinc oxide surface," *Superlattices Microstruct.*, vol. 39, no. 1–4, pp. 8–16, Jan.–Apr. 2006.
[41] D. B. Medved, "Photodesorption in zinc oxide semiconductor," *J. Chem. Phys.*, vol. 28, no. 5, pp. 870–873, May 1958.
[42] G. Heiland, "Homogeneous semiconducting gas sensors," *Sens. Actuators*, vol. 2, pp. 343–361, 1982.
[43] Q. Wan, Q. H. Li, Y. J. Chen, T. H. Wang, X. L. He, J. P. Li, and C. L. Lin, "Fabrication and ethanol sensing characteristics of ZnO nanowire gas sensors," *Appl. Phys. Lett.*, vol. 84, no. 18, pp. 3654–3656, May 2004.
[44] H. Nanto, T. Minami, and S. Takata, "Zinc-oxide thin-film ammonia gas sensors with high sensitivity and excellent selectivity," *J. Appl. Phys.*, vol. 60, no. 2, pp. 482–484, Jul. 1986.
[45] B. Xiang, P. Wang, X. Zhang, S. A. Dayeh, D. P. R. Aplin, C. Soci, D. Yu, and D. Wang, "Rational synthesis of p-type zinc oxide nanowire arrays using simple chemical vapor deposition," *Nano Lett.*, vol. 7, no. 2, pp. 323–328, 2007.
[46] A. Colli, A. Fasoli, P. Beecher, P. Servati, S. Pisana, Y. Fu, A. J. Flewitt, W. I. Milne, J. Robertson, C. Ducati, S. De Franceschi, S. Hofmann, and A. C. Ferrari, "Thermal and chemical vapor deposition of Si nanowires: Shape control, dispersion, and electrical properties," *J. Appl. Phys.*, vol. 102, no. 3, p. 034 302, Aug. 2007.
[47] H. Sirringhaus, T. Kawase, R. H. Friend, T. Shimoda, M. Inbasekaran, W. Wu, and E. P. Woo, "High-resolution Inkjet printing of all-polymer transistor circuits," *Science*, vol. 290, no. 5499, pp. 2123–2126, Dec. 2000.
[48] S. R. Forrest, "The path to ubiquitous and low-cost organic electronic appliances on plastic," *Nature*, vol. 428, no. 6986, pp. 911–918, Apr. 2004.
[49] Y. Sun, E. Menard, J. A. Rogers, H.-S. Kim, S. Kim, G. Chen, I. Adesida, R. Dettmer, R. Cortez, and A. Tewksbury, "Gigahertz operation in flexible transistors on plastic substrates," *Appl. Phys. Lett.*, vol. 88, no. 18, p. 183 509, May 2006.
[50] C. D. Dimitrakopoulos and P. R. L. Malenfant, "Organic thin film transistors for large area electronics," *Adv. Mater.*, vol. 14, no. 2, pp. 99–117, Jan. 2002.
[51] M. C. McAlpine, R. S. Friedman, and C. M. Lieber, "High-performance nanowire electronics and photonics and nanoscale patterning on flexible plastic substrates," *Proc. IEEE*, vol. 93, no. 7, pp. 1357–1363, Jul. 2005.
[52] X.-Z. Bo, C. Y. Lee, M. S. Strano, M. Goldfinger, C. Nuckolls, and G. B. Blanchet, "Carbon nanotubes–semiconductor networks for organic electronics: The pickup stick transistor," *Appl. Phys. Lett.*, vol. 86, no. 18, p. 182 102, May 2005.
[53] S. H. Hur, C. Kocabas, A. Gaur, O. O. Park, M. Shim, and J. A. Rogers, "Printed thin-film transistors and complementary logic gates that use polymer-coated single-walled carbon nanotube networks," *J. Appl. Phys.*, vol. 98, no. 11, p. 114 302, Dec. 2005.
[54] S. Liu, S. C. B. Mannsfeld, M. C. LeMieux, H. W. Lee, and Z. Bao, "Organic semiconductor–carbon nanotube bundle bilayer field effect transistors with enhanced mobilities and high on/off ratios," *Appl. Phys. Lett.*, vol. 92, no. 5, p. 053 306, Feb. 2008.
[55] G. W. Hsieh, P. Beecher, F. M. Li, P. Servati, A. Colli, A. Fasoli, D. Chu, A. Nathan, B. Ong, J. Robertson, A. C. Ferrari, and W. I. Milne, "Formation of composite organic thin film transistors with nanotubes and nanowires," *Physica E*, vol. 40, no. 7, pp. 2406–2413, May 2008.
[56] A. Babel and S. A. Jenekhe, "High electron mobility in ladder polymer field-effect transistors," *J. Amer. Chem. Soc.*, vol. 125, no. 45, pp. 13 656–13 657, Nov. 2003.
[57] T. D. Anthopoulos, C. Tanase, S. Setayesh, E. J. Meijer, J. C. Hummelen, P. W. M. Blom, and D. M. de Leeuw, "Ambipolar organic field-effect transistors based on a solution-processed methanofullerene," *Adv. Mater.*, vol. 16, no. 23/24, pp. 2174–2179, Dec. 2004.
[58] C. Waldauf, P. Schilinsky, M. Perisutti, J. Hauch, and C. J. Brabec, "Solution-processed organic n-type thin-film transistors," *Adv. Mater.*, vol. 15, no. 24, pp. 2084–2088, Dec. 2003.
[59] E. J. Meujer *et al.*, "Solution-processed ambipolar organic field-effect transistors and inverters," *Nat. Mater.*, vol. 2, no. 10, pp. 678–682, Oct. 2003.
[60] M. Chikamatsu, S. Nagamatsu, Y. Yoshida, K. Saito, K. Yase, and K. Kikuchi, "Solution-processed n-type organic thin-film transistors with high field-effect mobility," *Appl. Phys. Lett.*, vol. 87, no. 20, p. 203 504, Nov. 2005.
[61] Z. Fan, J. C. Ho, Z. A. Jacobson, R. Yerushalmi, R. L. Alley, H. Razavi, and A. Javey, "Wafer-scale assembly of highly ordered semiconductor nanowire arrays by contact printing," *Nano Lett.*, vol. 8, no. 1, pp. 20–25, 2008.
[62] S. C. Lim, S. H. Kim, J. H. Lee, M. K. Kim, D. J. Kim, and T. Zyung, "Surface-treatment effects on organic thin-film transistors," *Synth. Met.*, vol. 148, no. 1, pp. 75–79, Jan. 2005.

Flora M. Li received the M.A.Sc. and Ph.D. degrees in electrical and computer engineering from the University of Waterloo, Waterloo, ON, Canada, in 2003 and 2008, respectively.

From 2005 to 2008, she was a Visiting Scientist with Xerox Research Centre of Canada (XRCC). From 2006 to 2008, she was an Academic Visitor with the University of Cambridge, Cambridge, U.K. She is currently with the Department of Electrical and Computer Engineering, University of Waterloo. She has been awarded a national Postdoctoral Fellowship (PDF) from the Natural Sciences and Engineering Research Council (NSERC) of Canada in 2008. She also received national postgraduate scholarships from NSERC, the International Student Scholarship from Ontario Centers of Excellence (OCE), and numerous other scholarship and awards. She is the coauthor of CCD image sensors in *Deep Ultraviolet* (Springer, 2005). Her research interests include thin-film technology and devices based on organic materials, nanomaterials, nanocomposites, and transparent conducting oxides for applications in large-area electronics and flexible electronics including displays, sensors, photovoltaic devices, circuits, and systems.

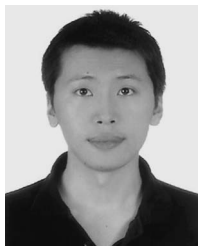

Gen-Wen Hsieh was born in Taiwan, in 1975. He received the B.S. degree in chemistry and the M.S. degree in chemical engineering from the National Tsing Hua University, Hsinchu, Taiwan, in 1999 and 2001, respectively. He is currently working toward the Ph.D. degree with the Electronic Devices and Materials Group, Electrical Engineering Division, University of Cambridge, Cambridge, U.K.

From 2002 to 2006, he was an R&D Engineer with the Industrial Technology and Research Institute (ITRI), Taiwan, where he worked on the fabrication of MEMS, NEMS, and flexible electronics. His research interests include 1-D nanomaterials, large-area self-assembly, and organic electronics.

Mr. Hsieh received the Overseas Research Studentship and Cambridge Overseas Trust Award in 2006.

Sharvari Dalal received the Ph.D. degree from the University of Cambridge, Cambridge, U.K.

She is currently with the Electronic Devices and Materials Group, Electrical Engineering Division, University of Cambridge, where she works on the synthesis and applications of ZnO nanowires.

Marcus C. Newton received the Ph.D. degree in nanoscale materials and devices from the University College London (UCL), London, U.K., in 2007.

He is currently with the London Centre for Nanotechnology, UCL, where he is involved in the use of computational phase reconstruction using data gathered from coherent X-ray diffraction measurements. This is used to determine 3-D structural changes due to strain in nanoscale crystals. His expertise lies in the study of II-VI heterostructures and quantum transport at semiconductor interfaces. He is also active in the study of semiconductor materials and the self-assembly of nanoscale crystal patterns for device integration.

James E. Stott received the B.A. (Hons.) and M.Eng. degrees in electrical and electronic engineering from the University of Cambridge, Cambridge, U.K., in June 2005. He is currently working toward the Ph.D. degree with the London Centre for Nanotechnology, University College London, London, U.K., where he is working on the design and integration of thin-film transistors and imaging arrays on flexible substrates. In his M.Eng. dissertation, he worked on the modeling and integration of microelectromechanical resonators for use in frequency reference applications.

In 2005, he was with ARM Ltd., U.K., where he worked on the design and verification of low-power audio DSPs for use in consumer electronic devices.

Pritesh Hiralal was born in Spain in 1980. He received the M.Phys. degree in physics in 2003 from the University of Manchester, Manchester, U.K., and the M.Phil. degree in microtechnology and nanotechnology enterprise in 2005 from the University of Cambridge, Cambridge, U.K., where he is currently working toward the Ph.D. degree.

His research interests include growth and electronic properties of 1-D materials, photovoltaics, and electrochemical devices.

Arokia Nathan received the Ph.D. degree in electrical engineering from the University of Alberta, Edmonton, Alberta, Canada, in 1988.

In 1987, he was with LSI Logic Corporation, Santa Clara, CA, where he worked on advanced multichip packaging techniques and related issues. Subsequently, he was with the Institute of Quantum Electronics, ETH Zürich, Zürich, Switzerland. In 1989, he was with the Department of Electrical and Computer Engineering, University of Waterloo, Waterloo, ON, Canada. In 1995, he was a Visiting Professor with the Physical Electronics Laboratory, ETH Zürich. In 1997, he was the DALSA/NSERC Industrial Research Chair in sensor technology and was a recipient of the 2001 Natural Sciences and Engineering Research Council E.W.R. Steacie Fellowship. In 2004, he was awarded the Canada Research Chair in nanoscale flexible circuits. In 2005/2006, he was a Visiting Professor with the Engineering Department, University of Cambridge, Cambridge, U.K. Since 2006, he has been with the London Centre for Nanotechnology, University College London, London, U.K., where he holds the Sumitomo/STS Chair of Nanotechnology. He is also the CTO of Ignis Innovation Inc., Waterloo, ON, Canada, a company he founded to commercialize technology on thin-film silicon backplanes on rigid and flexible substrates for large-area electronics. He has extensively published in the field of sensor technology and CAD, and thin-film transistor electronics, and has over 40 patents filed/awarded. He is the coauthor of two books *Microtransducer CAD* and *CCD Image Sensors in Deep-Ultraviolet* (Springer, 1999 and 2005, respectively).

Dr. Nathan serves on technical committees and editorial boards at various capacities. He was the recipient of the Royal Society Wolfson Research Merit Award.

Paul A. Warburton received the M.A. and Ph.D. degrees from the University of Cambridge, Cambridge, U.K., in 1994.

Following a period as a Research Fellow with the University of Maryland, College Park, he joined the academic staff at King's College London, London, U.K., in 1995. In 2001, took a lectureship in electrical engineering with the University College London, London, U.K. He is currently a Senior Lecturer with the London Centre for Nanotechnology, University College London. He held the Caius College Roberts Studentship and won the IEE Hudswell Bequest Scholarship at the University of Cambridge. He is the author or coauthor of over 50 peer-reviewed articles in academic journals. He is the director of the EPSRC "Access" U.K. national facility for focussed ion-beam nanofabrication and frequently acts as Expert Reviewer for the EU's programmes on quantum computation. His areas of research interest include superconductivity, Josephson junctions, nanofabrication using focussed ion beams, and semiconductor nanoparticles.

Dr. Warburton is a Chartered Physicist and a Member of the Institute of Physics and the IET. He has been the Technical Editor of the IEEE TRANSACTIONS ON APPLIED SUPERCONDUCTIVITY and was the Chairman of the "Plasma 2006" conference in London.

Husnu Emrah Unalan received the B.S. degree in metallurgical and materials science and engineering from the Middle East Technical University, Ankara, Turkey, in 2002 and the M.S. and Ph.D. degrees in materials science and engineering from Rutgers University, Piscataway, NJ, in 2004 and 2006, respectively.

He is currently with the Electrical Engineering Division, Engineering Department, University of Cambridge, Cambridge, U.K. His research interests include synthesis of nanotubes/nanowires and their utilization in large-area electronics and energy-harvesting devices.

Dr. Unalan was the recipient of the MRS Graduate Student Silver Award in 2005.

Paul Beecher received the B.E. (Elec., Hons.) degree in electrical engineering from the University College Cork, Cork, Ireland, and the Ph.D. degree in microelectronics from Tyndall National Institute, UCC, Cork.

He was a Research Associate with a particular interest in flexible and transparent electronics with the Engineering Department, University of Cambridge, Cambridge, U.K. He is currently a Senior Research Engineer with the Nokia Research Centre, Cambridge, U.K.

Andrew J. Flewitt received the B.Sc. degree in physics from the University of Birmingham, Birmingham, U.K., in 1994 and the Ph.D. degree in scanning tunneling microscopy of amorphous silicon from the University of Cambridge, Cambridge, U.K., in 1998.

He was a Research Associate studying the low-temperature growth of silicon-based materials with the Engineering Department, University of Cambridge, where he was a University Lecturer in 2002 and has been a Senior Lecturer since 2006, with a particular research interest in large-area electronic and microsystem devices.

Dr. Flewitt is a Chartered Physicist and a Member of the Institute of Physics and the Institution of Engineering and Technology.

Ian Robinson specializes in X-ray diffraction of materials using synchrotron radiation. He was previously with Bell Labs, where he developed methods for studying surface structure using X-ray diffraction. These methods, based on crystal truncation rods, have become the definitive technique for the determination of atomic positions at surfaces and interfaces. The surface methods are still used today at major SR facilities, NSLS (Brookhaven), ESRF (Grenoble), APS (Chicago), and SRS (Daresbury). More recently, he has been developing a method of using the very high coherence of the latest SR sources to enable direct 3-D imaging of structure. This is potentially useful for examining strain distributions inside complex materials. The coherent X-ray diffraction methods are being further expanded with the construction of a dedicated beamline at the new Diamond Light Source, Rutherford Laboratory, Oxford, U.K. He is currently with the University College London, London, U.K.

Gehan Amaratunga received the B.Sc. degree in electrical/electronic engineering from Cardiff University, Wales, U.K., in 1979 and the Ph.D. degree in electrical/electronic engineering from the University of Cambridge, Cambridge, UK., in 1983.

He currently heads the electronics, power and energy conversion group, one of four major research groups within the Electrical Engineering Division, Cambridge Engineering Faculty, University of Cambridge. He has worked on integrated and discrete electronic devices for power conversion for 23 years, and on the science and technology of carbon-based electronics for 20 years. He has published over 450 research articles in journals and conference proceedings. His research interests include nanoscale materials and device design for electronics and energy conversion; novel materials and device structures for low-cost highly efficient solar cells; power electronics for optimum grid connection of large photovoltaic electric generation systems; and integrated and discrete semiconductor devices for power switching and control.

Prof. Amaratunga is a Fellow of the Institute of Electrical Engineers and a Chartered Engineer. He was elected a Fellow of the Royal Academy of Engineering in 2004. Then, in 2007, he was awarded the Royal Academy of Engineering Silver Medal "for outstanding personal contributions to British Engineering."

William I. Milne received the B.Sc. degree from St. Andrews University, St Andrews, U.K., in 1970, the Ph.D. and DIC degrees in electronic materials from Imperial College, London, U.K., in 1973, and the D.Eng. (Honoris Causa) degree from the University of Waterloo, Waterloo, ON, Canada, in 2003.

From 1973 to 1976, he was with the Plessey Research Company, after which he w as an Assistant Lecturer with the Engineering Department, University of Cambridge, Cambridge, U.K. He has been the Head of electrical engineering since 1999 and Head of the Electronic Devices and Materials Group since 1996 with the University of Cambridge. His research interests include large-area Si and carbon-based electronics, thin-film materials, and, most recently, microelectromechanical systems (MEMS) and carbon nanotubes for electronic applications. He collaborates with various companies in these areas including Dow-Corning, Thales, Philips, Samsung, FEI, and NS3, and is currently involved in four European Union projects and several Engineering and Physical Sciences Research Council (EPSRC) projects. He has published/presented $\sim$500 papers in these areas.